



Transmittance-based Extinction and Viewpoint Optimization

Additional Material

Paul Himmler  and Tobias Günther 

Friedrich-Alexander-Universität Erlangen-Nürnberg, Germany

1. Derivation of the Functional Derivatives

We defined the energy $\mathcal{F}[\mu_t(\mathbf{x}), \mathbf{g}_V(\mathbf{x})] = \mathcal{F}_p + \mathcal{F}_q + \mathcal{F}_r$ with

$$\mathcal{F}_p = \frac{p}{2} \int_{\mathcal{D}} (\mu_t(\mathbf{x}) - \bar{\mu}_t(\mathbf{x}))^2 d\mathbf{x} \quad (1)$$

$$\mathcal{F}_q = -q \int_{\mathcal{D}} g(\mathbf{x}) \cdot \mu_t(\mathbf{x}) \cdot T_V(\mathbf{g}_V(\mathbf{x})) d\mathbf{x} \quad (2)$$

$$\mathcal{F}_r = -r \int_{\mathcal{D}} g(\mathbf{x}) \cdot \mu_t(\mathbf{x}) \cdot T_L(\mathbf{g}_L(\mathbf{x})) d\mathbf{x} \quad (3)$$

subject to the constraint $0 \leq \mu_t(\mathbf{x}) \leq \bar{\mu}_t : \forall \mathbf{x} \in \mathcal{D}$.

Differentiating Eq. (1) with respect to $\mu_t(\mathbf{x})$ gives:

$$\frac{\delta \mathcal{F}_p}{\delta \mu_t} = p \int_{\mathcal{D}} (\mu_t(\mathbf{x}') - \bar{\mu}_t(\mathbf{x}')) \cdot \frac{\delta \mu_t(\mathbf{x}')}{\delta \mu_t(\mathbf{x})} d\mathbf{x}' \quad (4)$$

$$= p \int_{\mathcal{D}} (\mu_t(\mathbf{x}') - \bar{\mu}_t(\mathbf{x}')) \cdot \delta(\mathbf{x}', \mathbf{x}) d\mathbf{x}' \quad (5)$$

$$= p \cdot (\mu_t(\mathbf{x}) - \bar{\mu}_t(\mathbf{x})) \quad (6)$$

In Eq. (4), the derivative $\frac{\delta \mu_t(\mathbf{x}')}{\delta \mu_t(\mathbf{x})} = \delta(\mathbf{x}', \mathbf{x})$ is a Dirac delta, leading to Eq. (5). By the sifting property of the Dirac delta, this simplifies to Eq. (6), as used in the paper.

Differentiating Eq. (2) with respect to $\mu_t(\mathbf{x})$ gives:

$$\frac{\delta \mathcal{F}_q}{\delta \mu_t(\mathbf{x})} = -q \int_{\mathcal{D}} g(\mathbf{x}') \cdot \left(\frac{\delta \mu_t(\mathbf{x}')}{\delta \mu_t(\mathbf{x})} \cdot T_V(\mathbf{g}_V(\mathbf{x}')) \right. \quad (7)$$

$$\left. + \mu_t(\mathbf{x}') \cdot \frac{\delta T_V(\mathbf{g}_V(\mathbf{x}'))}{\delta \mu_t(\mathbf{x})} \right) d\mathbf{x}' \quad (8)$$

$$= -q \int_{\mathcal{D}} g(\mathbf{x}') \cdot \frac{\delta \mu_t(\mathbf{x}')}{\delta \mu_t(\mathbf{x})} \cdot T_V(\mathbf{g}_V(\mathbf{x}')) d\mathbf{x}' \quad (9)$$

$$- q \int_{\mathcal{D}} g(\mathbf{x}') \cdot \mu_t(\mathbf{x}') \cdot \frac{\delta T_V(\mathbf{g}_V(\mathbf{x}'))}{\delta \mu_t(\mathbf{x})} d\mathbf{x}' \quad (10)$$

$$= -q \int_{\mathcal{D}} g(\mathbf{x}') \cdot \delta(\mathbf{x}', \mathbf{x}) \cdot T_V(\mathbf{g}_V(\mathbf{x}')) d\mathbf{x}' \quad (11)$$

$$+ q \int_{\mathcal{D}} g(\mathbf{x}') \cdot \mu_t(\mathbf{x}') \cdot T_V(\mathbf{g}_V(\mathbf{x}')) d\mathbf{x}' \quad (12)$$

$$= -q \cdot g(\mathbf{x}) \cdot T_V(\mathbf{g}_V(\mathbf{x})) \quad (13)$$

$$+ q \cdot \int_{\mathcal{D}} g(\mathbf{x}') \cdot \mu_t(\mathbf{x}') \cdot T_V(\mathbf{g}_V(\mathbf{x}')) d\mathbf{x}' \quad (14)$$

$$= q \cdot (G_V(\mathbf{g}_V(\mathbf{x})) - g(\mathbf{x}) \cdot T_V(\mathbf{g}_V(\mathbf{x}))) \quad (15)$$

Eqs. (7)–(8) followed from the chain rule. Expanding the integral into two terms gives Eqs. (9)–(10). Note that the integration in Eq. (10) changed from a volume integral to a line integral, since the transmittance is only affected by variations of the extinction along the view ray and is zero everywhere else. Substituting the Dirac delta in Eq. (9) leads to Eq. (11), which simplifies by sifting to Eq. (13). The step from Eq. (10) to Eq. (12) requires the functional derivative of the transmittance T_V with respect to extinction $\mu_t(\mathbf{x})$:

$$\frac{\delta T_V(\mathbf{y})}{\delta \mu_t(\mathbf{x})} = T_V(\mathbf{y}) \cdot \left(-\frac{\delta}{\delta \mu_t(\mathbf{x})} \int_{y_0}^y \mu_t(\mathbf{g}_V^{-1}(\mathbf{y}')) d\mathbf{y}' \right) \quad (16)$$

$$= T_V(\mathbf{y}) \cdot \left(-\int_{y_0}^y \frac{\delta \mu_t(\mathbf{g}_V^{-1}(\mathbf{y}'))}{\delta \mu_t(\mathbf{x})} d\mathbf{y}' \right) \quad (17)$$

$$= T_V(\mathbf{y}) \cdot \left(-\int_{y_0}^y \delta(\mathbf{g}_V^{-1}(\mathbf{y}'), \mathbf{x}) d\mathbf{y}' \right) \quad (18)$$

$$= -T_V(\mathbf{y}) \quad (19)$$

Eq. (16) arises from the application of the chain rule in the definition of the transmittance:

$$T_V(\mathbf{y}) = e^{-\int_{y_0}^y \mu_t(\mathbf{g}_V^{-1}(\mathbf{y}')) d\mathbf{y}'} \quad (20)$$

Eq. (17) moves the differentiation with the Leibniz rule into the integral. Again a Dirac delta is substituted for Eq. (18), resulting in Eq. (19). The differentiation of Eq. (3) with respect to $\mu_t(\mathbf{x})$ is analogous.

Lastly, the derivative of Eq. (2) with respect to the cameras rotation angles α_i is given by:

$$\frac{\delta \mathcal{F}_q}{\delta \alpha_i} = -q \int_{\mathcal{D}} g(\mathbf{x}) \cdot \mu_t(\mathbf{x}) \cdot \frac{\delta T_V(\mathbf{g}_V(\mathbf{x}))}{\delta \alpha_i} d\mathbf{x} \quad (21)$$

Eq. (21) requires the functional derivative of the transmittance T_V

with respect to the cameras rotation angles α_i :

$$\frac{\delta T_V(\mathbf{g}_V(\mathbf{x}))}{\delta \alpha_i} = -T_V(\mathbf{g}_V(\mathbf{x})) \cdot \int_{y_0}^y \frac{\delta \mu_t(\mathbf{y}')}{\delta \alpha_i} d\mathbf{y}' \quad (22)$$

$$= -T_V(\mathbf{g}_V(\mathbf{x})) \cdot \int_{y_0}^y \frac{\delta \mu_t(\mathbf{g}_V^{-1}(\mathbf{y}'))}{\delta \mathbf{g}_V^{-1}(\mathbf{y}')} \frac{\delta \mathbf{g}_V^{-1}(\mathbf{y}')}{\delta \alpha_i} d\mathbf{y}' \quad (23)$$

$$= -T_V(\mathbf{g}_V(\mathbf{x})) \cdot \int_{y_0}^y \nabla \mu_t(\mathbf{g}_V^{-1}(\mathbf{y}')) \frac{\delta \mathbf{g}_V^{-1}(\mathbf{y}')}{\delta \mathbf{y}'} \frac{\delta \mathbf{y}'}{\delta \alpha_i} d\mathbf{y}' \quad (24)$$

where

$$\frac{\delta \mathbf{g}_V^{-1}(\mathbf{y}')}{\delta \mathbf{y}'} = \mathbf{R} \cdot (\hat{\mathbf{u}}, \hat{\mathbf{v}}, \hat{\mathbf{w}}) \quad (25)$$

and

$$\hat{\mathbf{u}} = \mathbf{u} \cdot (z_n + y'_3(z_f - z_n)) \quad (26)$$

$$\hat{\mathbf{v}} = \mathbf{v} \cdot (z_n + y'_3(z_f - z_n)) \quad (27)$$

$$\hat{\mathbf{w}} = (y'_1 \cdot \mathbf{u} + y'_2 \cdot \mathbf{v} + \mathbf{w}) \cdot (z_f - z_n) \quad (28)$$

2. Parameter Study

Our energy consists of three terms that each have their respective energy weight. Since a uniform scaling of the weights leads to an identical minimum, the energy weights can be restricted by normalization, for which we set the regularization term to $p = 10^{-3}$. This term has a small weight, such that it does not contribute in regions where the other terms operate, i.e., where occlusions occur. In the following, we study the effect of the energy weights q and r in Eqs. (2)–(3). Fig. 1 shows that varying the weights has an intuitive impact. The higher the weight q , the more important regions become visible. For small weights, important structures might be missed, while a large weight also emphasizes structures with medium importance. The higher the weight r , the better is the light path cleared to illuminate the interesting regions. While a small weight results in important parts being poorly illuminated, increasing the weight initially illuminates the important parts well, but eventually overexposes them by illuminating less important parts in their neighborhood. Apart from the parameter study, in which the weights have been altered deliberately, we used the same weights of $q = 10$ and $r = 1$ across all images in the paper, which shows that no parameter tuning was necessary in the considered test scenes.

3. Informal User Study

We conducted an informal user study in which 9 researchers from visual computing (with 6 months to 6 years of professional experience) ranked the visualizations in Fig. 8 of the main paper by considering the following questions:

- How well is relevant information conveyed?
- How well is depth perception supported?
- How well is the shading maintained?

Participants ranked the methods from worst (4) to best (1). Since Viola et al. [VKG04] and Marchesin et al. [MMD10] did not incorporate shadowing, we compare all methods first without shadowing.

Afterwards, Ament et al. [AZD17] and our method are compared with shadowing. The detailed results are listed in Table 1. In the following, we elaborate on the observations we made from the feedback of the participants.

Results of Viola et al. [VKG04] In the study, users observed a lack of details in the method of Viola et al. Although this was noted in all datasets, it was particularly noticeable in the VISIBLE HUMAN and HEPTANE FLAME datasets. In the case of the former, it was also frequently noted that the lack of consistency of the selected important elements in the cranial surface significantly reduces the visual quality and that the perception of depth is inhibited due to these artifacts. Although this criticism also occurred for the other datasets, it was not perceived as too disturbing for some of them.

Results of Marchesin et al. [MMD10] The method of Marchesin et al. was often assessed positively at first glance. However, points of criticism were that the often blurred contours impair the perception of depth and the color values do not match those of the standard rendering. The latter was often ignored in the final evaluation decision, as it is most visible in less important regions. Therefore, it was convincing in the HEPTANE FLAME data set, for example. The ranking placement of Marchesin et al. varies across the data sets.

Results of Ament et al. [AZD17] In many cases, users found the results of Ament et al. to be appealing. Compared to Viola et al. the better visualization of details was highlighted, while compared to Marchesin, the ability to distinguish between important and less important details was appreciated. The latter was the main reason why it was often preferred over these two methods. However, users frequently criticized the lack of some details they expected to see. This was mentioned especially in the VISIBLE HUMAN data set. Some users also pointed out color differences compared to the standard rendering in some cases. With the additional lighting optimization, the lack of detail in the extinction optimization was said to be even more obvious. In addition, the lighting appeared less optimized compared to the optimization we suggest.

Results of our Method On average our method was described as the best compromise of all evaluation criteria. The retention of the important details while maintaining a clear but visually appealing distinction between important and unimportant structures was emphasized several times. Depth perception, although generally difficult, was rated as the best by most participants. The preservation of colors compared to the standard rendering of the volume was also often mentioned as the best that can be achieved. The lighting optimization was praised for improving the depth perception even further. For the VISIBLE HUMAN data set, the details appearing on the skull were appreciated. The general appearance was rated as appealing and fulfilling the specified evaluation criteria.

4. Convergence Plots

Our extinction and viewpoint optimization both minimize the metric $\mathcal{F} = \mathcal{F}_p + \mathcal{F}_q + \mathcal{F}_r$. To quantitatively assess the visibility of relevant structures, however, we chose the visibility score \mathcal{S} , which is only the (negated and unweighted) term \mathcal{F}_q . This was done, because some of the competing methods we compared with do not perform

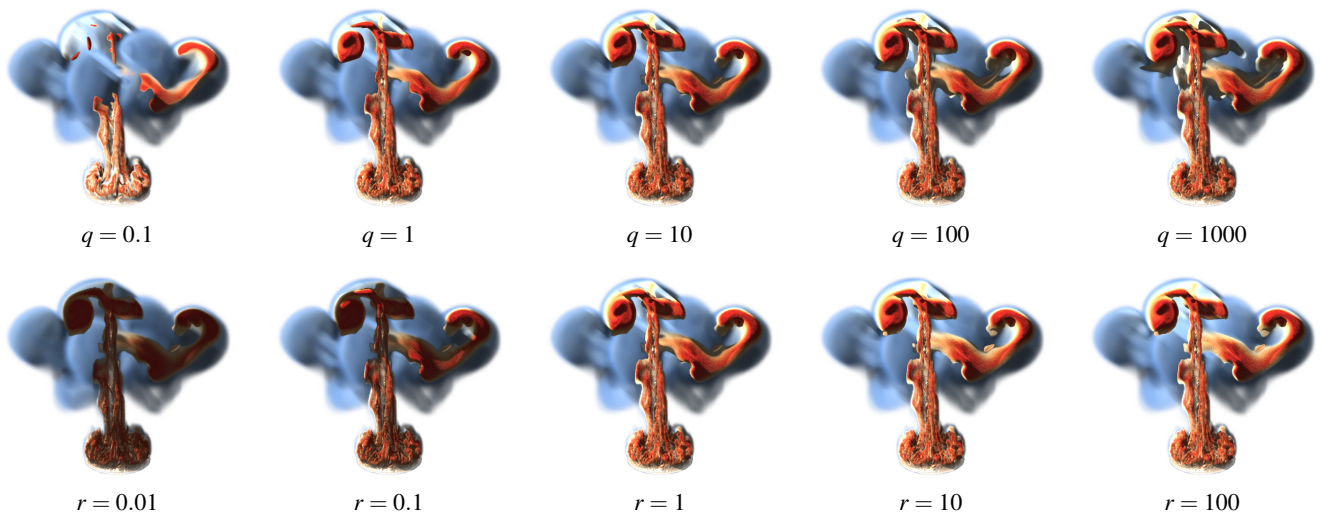


Figure 1: Variation of the energy weights q (in the first row) and r (in the second row). The recommended setting is in the middle column.

Participant	EARTH MANTLE						VISIBLE HUMAN						HEPTANE FLAME						ROTATING MIXER											
	[VKG04]	[MMD10]	[AZD17]	ours	[AZD17]	ours	[VKG04]	[MMD10]	[AZD17]	ours	[AZD17]	ours	[VKG04]	[MMD10]	[AZD17]	ours	[AZD17]	ours	[VKG04]	[MMD10]	[AZD17]	ours	[AZD17]	ours						
P1	3	4	2	1	4	1	4	3	2	1	4	1	4	3	2	1	4	1	3	4	2	1	4	1	3	4	2	1	4	1
P2	4	3	1	2	1	4	4	3	2	1	4	1	4	1	3	2	4	1	4	3	2	1	4	1	4	3	2	1	4	1
P3	3	4	2	1	1	4	4	2	3	1	4	1	4	1	3	2	4	1	4	3	2	1	4	1	4	1	3	2	4	1
P4	4	3	2	1	4	1	4	3	2	1	4	1	4	1	3	2	4	1	4	1	3	2	4	1	4	1	3	2	4	1
P5	3	4	2	1	4	1	4	2	3	1	4	1	4	1	3	2	4	1	4	1	3	2	4	1	4	1	3	2	4	1
P6	4	2	3	1	1	4	4	2	3	1	4	1	4	2	3	1	4	1	1	4	2	3	4	1	1	4	2	3	4	1
P7	2	4	3	1	4	1	2	4	3	1	4	1	4	1	3	2	4	1	3	1	4	2	4	1	3	1	4	2	4	1
P8	3	4	2	1	4	1	4	3	2	1	4	1	4	3	2	1	4	1	4	1	3	2	4	1	4	1	3	2	4	1
P9	4	1	3	2	4	1	2	1	3	2	4	1	4	1	3	2	4	1	4	2	3	1	4	1	4	2	3	1	4	1

Table 1: Results of the user study. For each of the four data sets, we compared [VKG04], [MMD10], [AZD17] and our method without shadowing (left), and [AZD17] and our method with shadowing (right). The users ranked the visualizations from 4 (worst) to 1 (best).

an extinction optimization on light rays, which is why \mathcal{F}_r would have been undefined. This, however, begs the question whether S and \mathcal{F} ultimately descent to the same optimum. In Fig. 2 we show convergence plots of our extinction optimizations in Fig. 8 in the paper to demonstrate the close correlation between the total energy \mathcal{F} (which is minimized) and our visibility score S (which is maximized).

5. Further Viewpoints for Comparison

In analogy to the results shown in Fig. 8 of the main paper, we provide further results for a different viewpoint in Figs. 3–6. Compared to the views shown in the main paper, the figures in the additional material show less optimal views with more occlusion. The extinction optimizations therefore result in lower visibility scores. Our proposed approach, however, consistently results in the highest

score, since it directly optimizes for the visibility metric \mathcal{F} , which is closely related to S , as was shown in the previous section.

References

- [AZD17] AMENT M., ZIRR T., DACHSBACHER C.: Extinction-optimized volume illumination. *IEEE Transactions on Visualization and Computer Graphics* 23, 7 (2017), 1767–1781. doi:10.1109/TVCG.2016.2569080. 2, 3, 5, 6
- [MMD10] MARCHESIN S., MONGENET C., DISCHLER J.: Per-pixel opacity modulation for feature enhancement in volume rendering. *IEEE Transactions on Visualization and Computer Graphics* 16, 04 (jul 2010), 560–570. doi:10.1109/TVCG.2010.30. 2, 3, 5, 6
- [VKG04] VIOLA I., KANITSAR A., GROLLER M.: Importance-driven volume rendering. In *IEEE Visualization 2004* (2004), pp. 139–145. doi:10.1109/VISUAL.2004.48. 2, 3, 5, 6

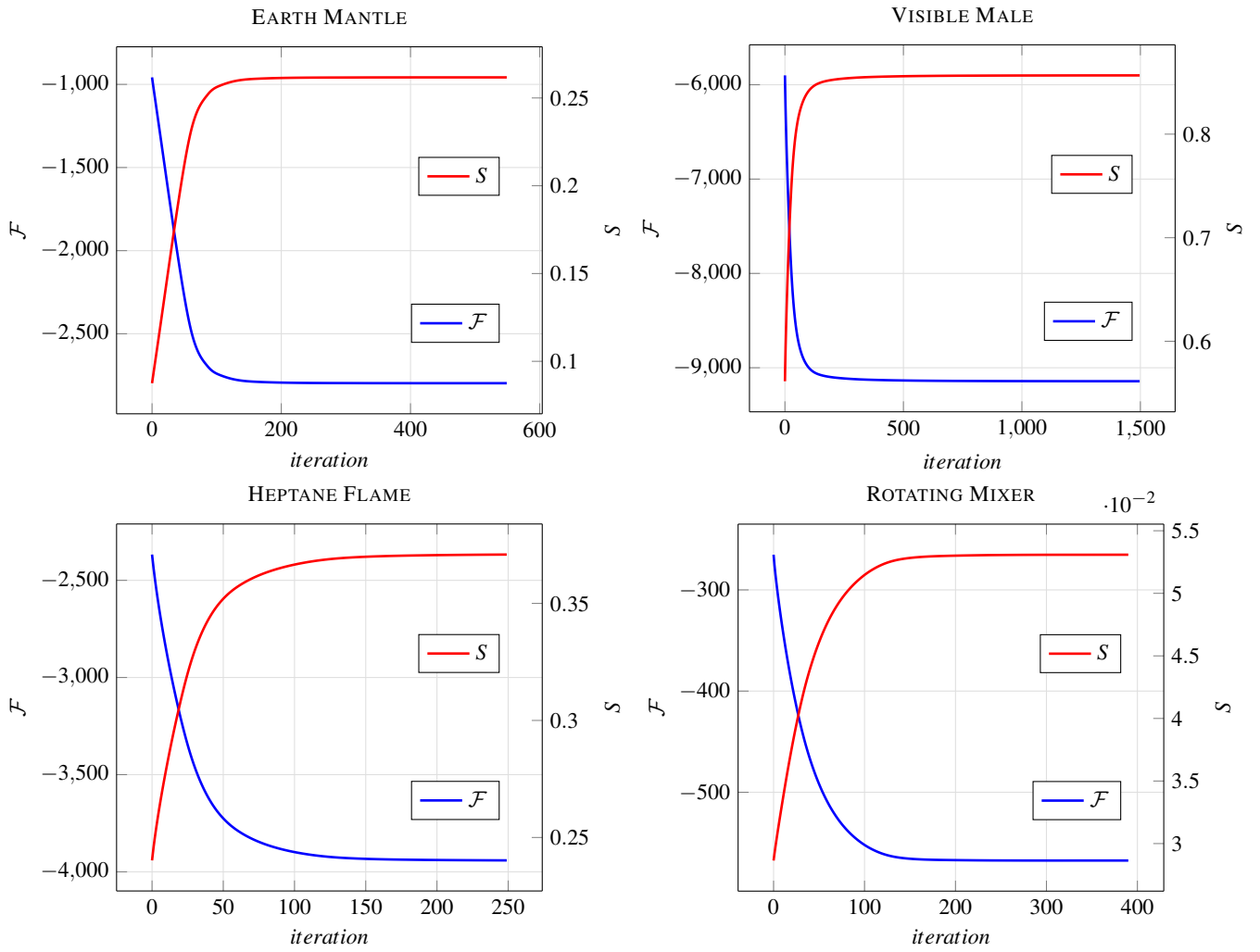


Figure 2: Convergence plots showing the score S and the total energy \mathcal{F} over the course of the extinction optimization.

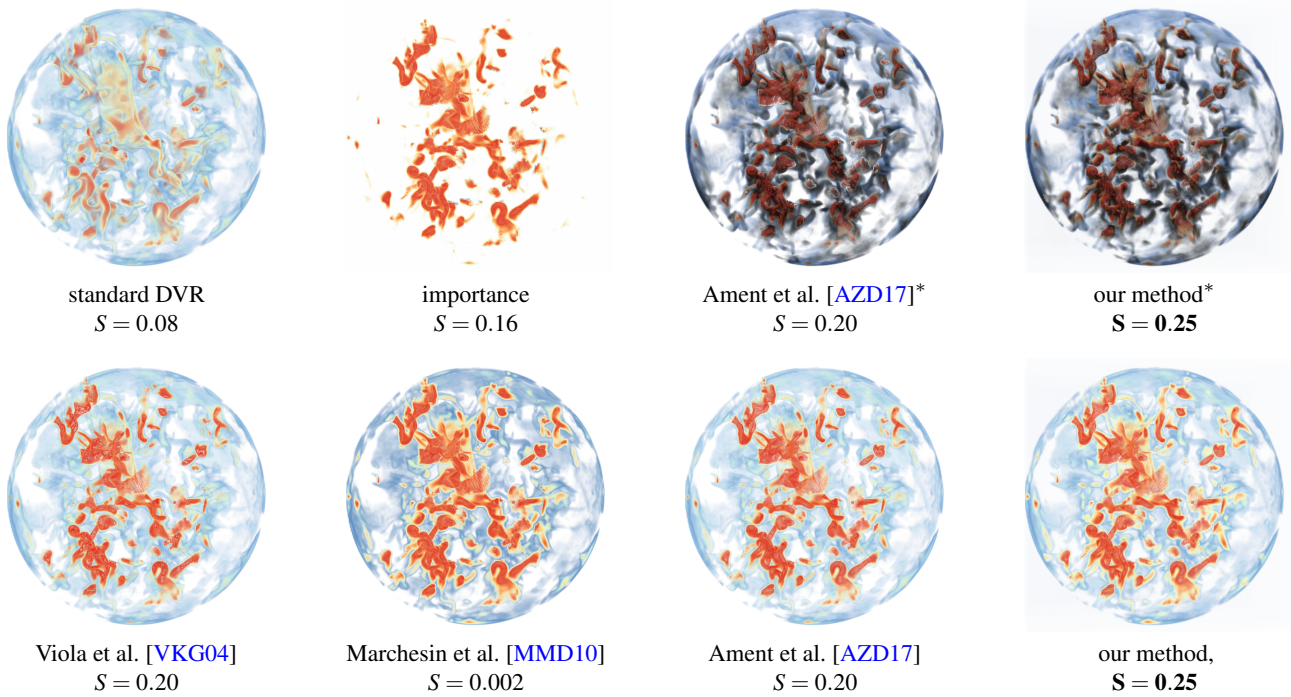


Figure 3: Comparison between the extinction optimization methods in the EARTH MANTLE data set. Images marked with a (*) are with shadowing, while the others are without shadowing. The visibility score S is listed for each method.

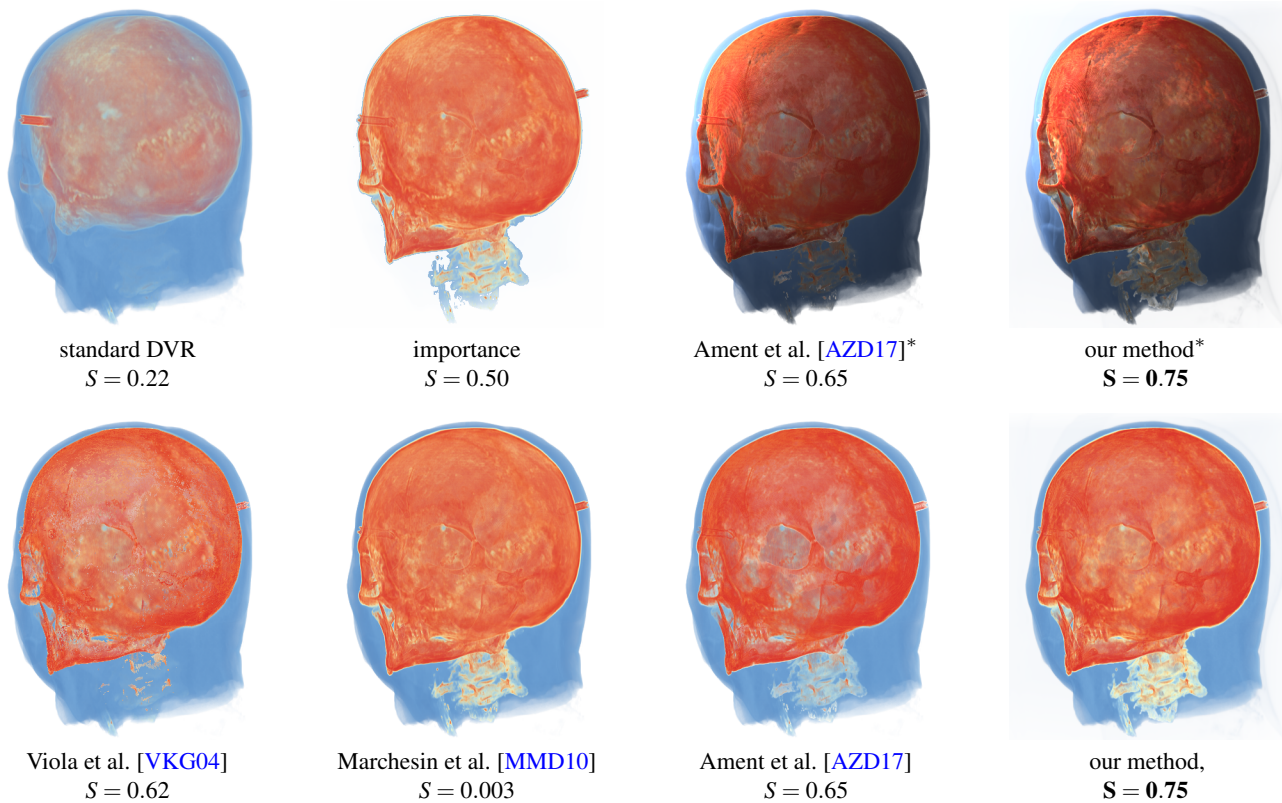


Figure 4: Comparison between the extinction optimization methods in the VISIBLE HUMAN data set. Images marked with a (*) are with shadowing, while the others are without shadowing. The visibility score S is listed for each method.

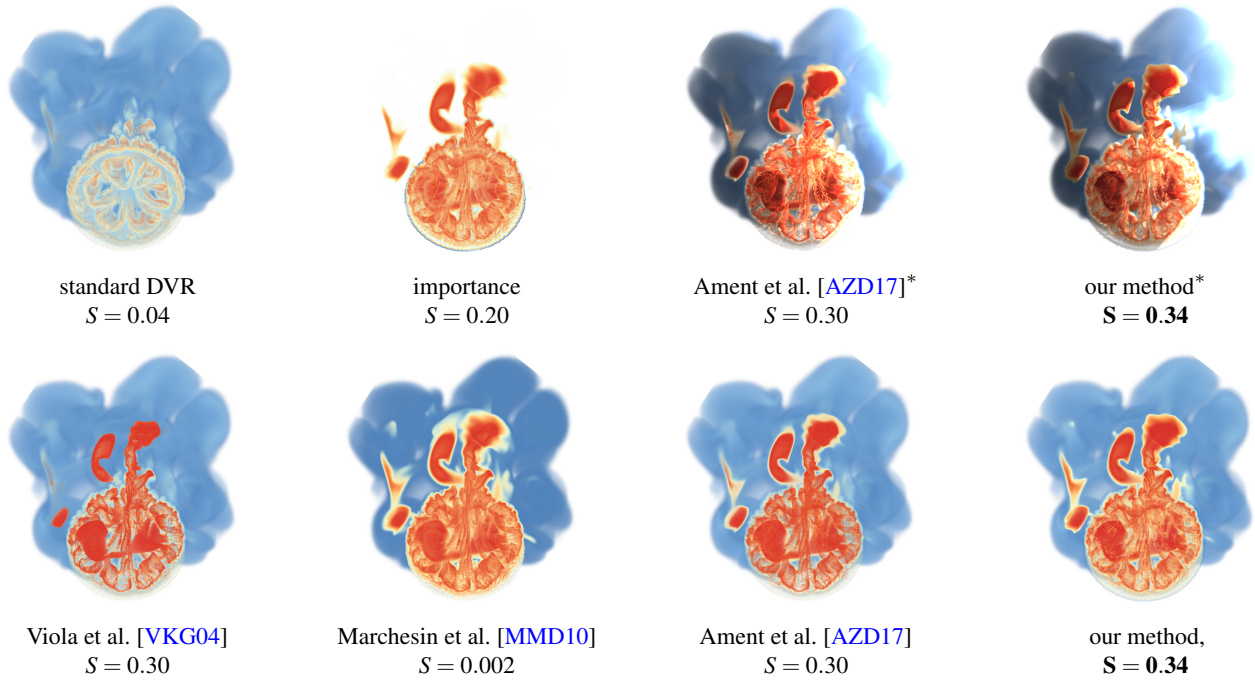


Figure 5: Comparison between the extinction optimization methods in the HEPTANE FLAME data set. Images marked with a (*) are with shadowing, while the others are without shadowing. The visibility score S is listed for each method.

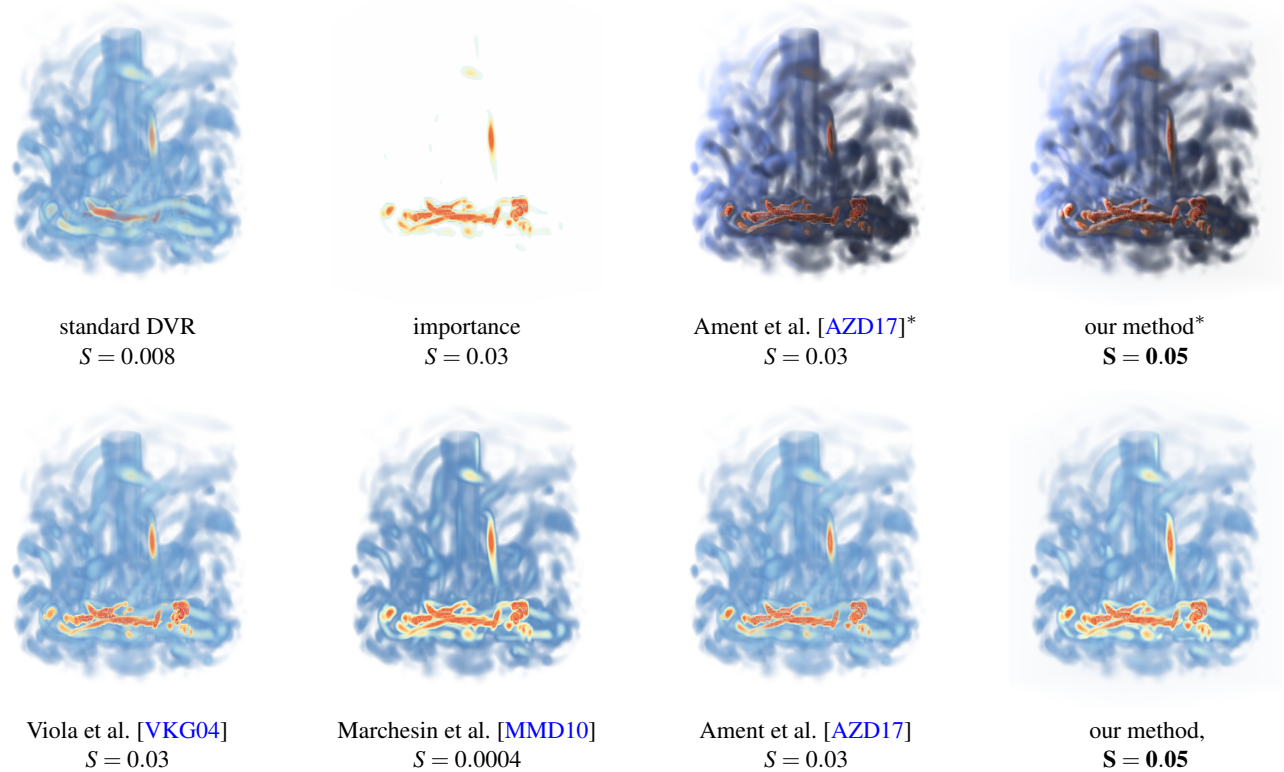


Figure 6: Comparison between the extinction optimization methods in the ROTATING MIXER data set. Images marked with a (*) are with shadowing, while the others are without shadowing. The visibility score S is listed for each method.